Journal of Molecular Graphics and Modelling 27 (2008) 244–254

Contents lists available at ScienceDirect

Journal of Molecular Graphics and Modelling

journal homepage: www.elsevier.com/locate/JMGM

Homology models of the mutated EGFR and their response towards quinazolin analogues

Sabitha Kotra [a], Kishore Kumar Madala [b], Kaiser Jamil [c,*]

[a] Mahavir Medical Research Center Hyderabad, AP India
[b] GVK Bio Science Pvt. Ltd., Bala Nagar, Hyderabad, AP India
[c] Indo American Cancer Institute & Research Centre, Road No. 14, Banjara Hills, Hyderabad 500034, AP, India

ARTICLE INFO

Article history:
Received 26 January 2008
Received in revised form 20 April 2008
Accepted 24 April 2008
Available online 3 May 2008

Keywords:
Affinity
Homology modeling
In silico
Docking
EGFR
Quinazolin
Gefitinib
Erlotinib
CI-1033
EKB-569
Mutation

ABSTRACT

One of the most intensely studied tyrosine kinases is the epidermal growth factor receptor (EGFR). The tyrosine kinase receptors are known to be over expressed in some solid tumors and non-small cell lung cancers, causing differential susceptibility to the quinazoline inhibitors. In this study we have taken SYK tyrosine kinase coordinates from PDB database to model two new EGFR receptors with these mutations G695S and L834R and conducted all the docking studies of the inhibitors, also evaluated these two models for quality of structure using PROCHECK. Seven quinazoline analogues (gefitinib, erlotinib, CI-1033, and EKB-569 and other analogues) were selected for comparisons among the two new models. This study determined the receptor/inhibitor interactions, at that active domain binding sites consisting of 15 amino acids. We were able to calculate the energy data for each of the seven inhibitors. This data has been important in interpreting the affinity between the inhibitors evaluated against the three models of EGFR (wild-type and two mutated types). "Affinity"-based studies have indicated the order of response based on docking energy levels (Van der Waals and electrostatic interactions). The active ATP binding sites consisting of 15 amino acid residues were identified and the total energy (E_{total}) which showed the affinity between the inhibitor molecules and the receptor (Van der Waals and electrostatic interactions). The selection of the quinazoline analogues was purely on their emergence as possible candidates in the drug discovery areas. This study describes the successful application of these models that we constructed for molecular docking studies to rationally design compounds predicted to bind favorably to the modeled EGFR catalytic sites.

1. Introduction

Increasing knowledge of the structure and function of the epidermal growth factor receptor (EGFR) subfamily of tyrosine kinases and their role in the initiation and progression of various cancers has lead to the search for inhibitors of these signaling molecules that may prove to be important in cancer therapy [1–5]. EGFR is a 170-kDa transmembrane glycoprotein and is composed of a glycosylated N-terminal, extra-cellular ligand binding region (621 residues), a hydrophobic transmembrane region (23 residues), and a C-terminal intracellular region (542 residues) which contains the tyrosine kinase domain (approximately 250 residues) [6,7]. The major sites of phosphorylation are located at the C-terminal tyrosine residues at positions 1068, 1086, 1148 and 1173.

A series of novel mutations have been reported in EGFR gene, which have affinity for quinazoline inhibitors in non-small cell lung cancer (NSCLC) [8,9]. Although gefitinib has been used for the treatment of NSCLCs, it was demonstrated that only those cells expressing EGFR mutations responded well to the treatment and had better and longer treatment and longer disease free survival [10,11]. Earlier our studies on single nucleotide polymorphisms in various genes like MTHFR, GSTs, CYP's, TS, and Mex-R which relate to dose response of neoplastic drugs in cancer patients have yielded interesting results in determining the susceptibility or overall survival in breast cancer cases, leukemia's and corneal keratitis.

Non-small cell lung cancer is the leading cause of death from cancer in both male and female patients. Chemotherapy, the mainstay of treatment in advanced cancers, is only marginally effective therapy, but gefitinib and erlotinib, which target the EGFR pathway, showed promise in the treatment of metastatic non-small cell lung cancer. Response rates as reported by Ref. [8] were 10–20% when these ATP-competitive anilinoquinazoline inhibitors

* Corresponding author. Tel.: +91 40 23540348; fax: +91 40 23542120.
E-mail addresses: sabitha_kotra@yahoo.com (S. Kotra), Kaiser.jamil@gmail.com (K. Jamil).

1093-3263/$ – see front matter © 2008 Elsevier Inc. All rights reserved.
doi:10.1016/j.jmgm.2008.04.010

were used as second or third line of treatment for advanced disease. Responsiveness to these drugs is a characteristic of distinct subgroups of patients such as women patients who never smoked, patients with adenocarcinomas and some Asians. In the majority of patients with highly responsive tumors, somatic mutations of the EGFR gene was seen in the tumor samples. These mutations are small deletions that affect amino acids 747 through 750 or point mutations, most commonly a replacement of leucine by arginine at codon 834 (L834R) and glycine by serine at codon 695 (G695S).

Many human malignancies exhibit mutated forms of the EGFR, a tyrosine kinase that plays a critical role in signaling pathways controlling cell proliferation and survival. Although the specific mechanisms are unclear, studies have shown that some EGFR mutations are associated with increased sensitivity to small-molecule tyrosine kinase inhibitors. To better understand how distinct mutant EGFRs interact with inhibitors on a structural level, we designed the two lung cancer-derived EGFR mutants and determined their structures by homology modeling, and used these two models to study the seven analogues of quinazoline inhibitors [12] (Fig. 1).

The common mutations (G695S and L834R) can induce oncogenic effects by altering the downstream signaling and anti-apoptotic mechanisms [8], However, these mutations in NSLC's have shown changes in the response of the tumor to anilinoquinazoline inhibitors [12], by repositioning critical residues surrounding the ATP-binding cleft of the tyrosine kinase domain of the receptor, thereby stabilizing their interactions with both ATP and its competitive inhibitors.

In order to check the importance of the receptor ligand interactions, our objective was to evaluate the best possible combination for targeted therapies using tyrosine kinase receptor of EGFR as target against the known quinazolines analogues which have been designated as promising compounds for therapy. The choice of quinazoline inhibitors selected for this study was those that could enter clinical trials and more promising ligands [13–18].

2. Materials and methods

2.1. Databases, equipment, and software

Using various database like EMBL, GenBank, and Swiss-Prot (U48723, NM_005228, and P00533) we obtained the EGFR sequence for this study. The crystal structure of EGFR was obtained from PDB (1M17.pdb). Mutation analysis, model building, and all in silico studies were carried out on Silicon Graphics Octane and O2 workstations (Silicon Graphics Inc., Mountain View, CA). Insight II 98.0 software from Accelrys was used in the protein homology modeling and PROCHECK for structure validation. The software utilized in the computational analysis was GRID. Chemical structures (compounds 1–7) were imported from ISIS-BASE database or drawn in ISIS-Draw (MDL information Systems Inc., San Leandro, CA), further affinity studies were performed with these structures using various software's as described below. Energy minimizations were carried out wherever required for accurate predictions.

2.2. Protein homology modeling

The crystal structure of SYK tyrosine kinase domain was used as primary template for modeling the mutated EGFR (L834R and G695S, Fig. 2). The sequence identity between SYK tyrosine kinase and EGFR (from PDB) was 64% which makes SYK tyrosine kinase domain a good template for modeling the two new mutated EGFR structures used in this study. The modeling was carried out with the Insight II Modeller module [19,20].

These two new models were then tested for their structure similarities, using Blast and ClustalW and were found to have domain similarity with the SYK tyrosine kinase–ATP-binding domain. This was further confirmed by plotting it on the Ramachandran plot and the values showed the best quality of the structure that we modeled.

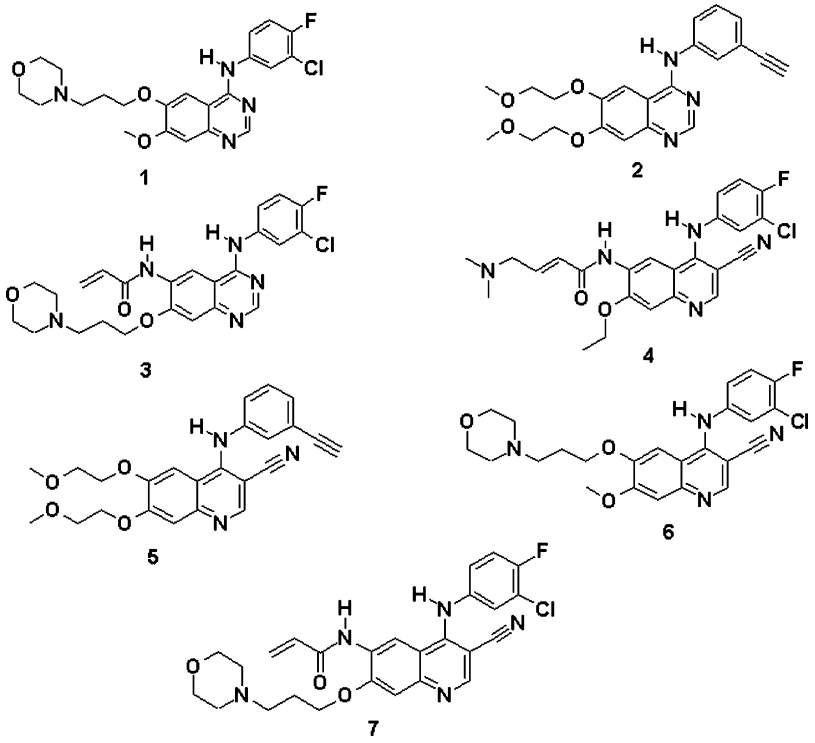

Fig. 1. Quinazoline inhibitors. (Quinazoline analogues, inhibitors) **1** (Gefitinib), **2** (Eltronib), **3** (CI-1033), **4** (EKB-569), and **5**–**7** (analogues of quinazoline).

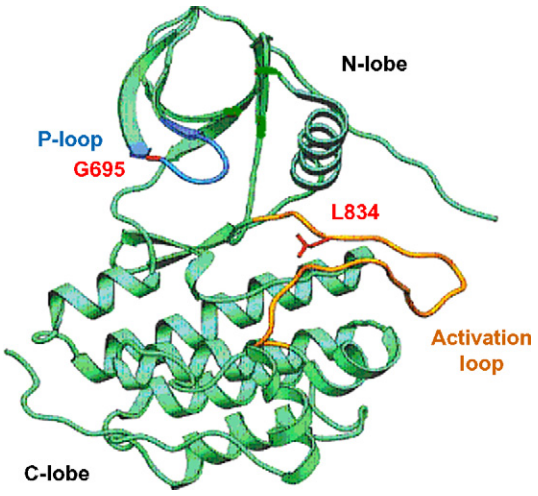

Fig. 2. Position of missense mutations G695S and L834R in EGFR structure.

2.3. Sequence alignment

Amino acid sequence of EGFR was obtained from Swiss-Prot [21] database, accession no. P00533. Sequence homology searches were carried out using BLAST [22] algorithm against Protein data bank. Target–template alignment was created using ALIGN2D command of 'Modeller' which implements a global dynamic algorithm with a variable gap penalty. Modeling was carried out selecting 1XBC (SYK tyrosine kinase domain with the inhibitor complex) [23] as the primary template. Both share a sequence similarity 64% to enhance the quality of protein in terms of the structurally conserved regions and structurally variable regions. We selected ABL kinase domain (1FPU.pdb) [24], human lymphocyte kinase (3LCK.pdb) [25] and tyrosine kinase domain of the human insulin receptor (1IRK.pdb) [26] as secondary templates. Sequence alignment of all the sequences was performed using ClustalW [27] (Fig. 3). These sequences were at first manually aligned and then submitted to 'Modeller' for further automation.

2.4. Model building

The three-dimensional new models of EGFR (with mutated sequences) was constructed using crystal structure coordinates of SYK tyrosine kinase (1XBC.pdb) as primary template using the program 'Modeller' [28,29]. 'Modeller' is a computer program that models three-dimensional structures of proteins and their assemblies by satisfying of spatial restraints. 'Modeller' is most frequently used for homology or comparative protein structure modeling. The alignment of the sequence obtained from ClustalW (Fig. 3) was taken as input for the 'Modeller' for modeling the new structure with mutations (1XBC.pdb, was our primary template and 1FPU.pdb was the secondary template). The 'Modeller' automatically calculates and binds the model with all non-hydrogen atoms. More generally, the inputs to the program were restrained on the spatial structure of the amino acid sequence(s) to be modeled. The output of 'Modeller' was the 3D structure of the protein that satisfied these restraints in the best possible manner. 'Modeller' automatically derives the restraints from the known related structures and their alignment with the target sequence. A 3D model was obtained by optimization of a molecular probability density function (pdf). The molecular pdf for comparative modeling was optimized with the variable target function procedure in Cartesian space that employs methods to conjugate gradients and molecular dynamics with simulated annealing. The two new models thus obtained were evaluated with PROCHECK.

2.5. Evaluation of the models by PROCHECK

The quality of the models obtained as above was evaluated by PROCHECK [30]. PROCHECK indicates the percentage of residues located in the favored regions of the Ramachandran plot. This plot

```
1M17_A|SEQUENCE    GSHMASGEAPNQALLRILKETEFKKIKVLGSGAFGTVYKGLWIPEGEKVKIPVAIKELR- 59
1FPU_A|SEQUENCE    GAMDPS--SPNYDKWEMER-TDITMKHKLGGGQYGEVYEGVWK----KYSLTVAVKTLK- 52
1XBC_A|SEQUENCE    --MALEEIRPKE--VYLDRKLLTLEDKELGSGNFGTVKKGYYQMK--KVVKTVAVKILKN 54
                         .   *:     : :       : **.* :* * :* :     *   .**:* *:

1M17_A|SEQUENCE    EATSPKANKEILDEAYVMASVDNPHVCRLLGICLTS-TVQLITQLMPFGCLLDYVREH-K 117
1FPU_A|SEQUENCE    EDT--MEVEEFLKEAAVMKEIKHPNLVQLLGVCTREPPFYIITEFMTYGNLLDYLRECNR 110
1XBC_A|SEQUENCE    EANDPALKDELLAEANVMQQLDNPYIVRMIGICEAE-SWMLVMEMAELGPLNKYLQQN-- 111
                   * .     .*:* ** ** .:.:* : :::*:*  . .  :: ::   * * .*:::

1M17_A|SEQUENCE    DNIGSQYLLNWCVQIAKGMNYLEDRRLVHRDLAARNVLVKTPQHVKITDFGLAKLLGAEE 177
1FPU_A|SEQUENCE    QEVSAVVLLYMATQISSAMEYLEKKNFIHRDLAARNCLVGENHLVKVADFGLSRLMTGDT 170
1XBC_A|SEQUENCE    RHVKDKNIIELVHQVSMGMKYLEESNFVHRDLAARNVLLVTQHYAKISDFGLSKALRADE 171
                    .:    ::    *:: .*:***. .::******** *:   : .*::****:: : .:

1M17_A|SEQUENCE    KEYHAE-GGKVPIKWMALESILHRIYTHQSDVWSYGVTVWELMTFGSKPYDGIPASEISS 236
1FPU_A|SEQUENCE    YTAHA--GAKFPIKWTAPESLAYNKFSIKSDVWAFGVLLWEIATYGMSPYPGIDLSQVYE 228
1XBC_A|SEQUENCE    NYYKAQTHGKWPVKWYAPECINYYKFSSKSDVWSFGVLMWEAFSYGQKPYRGMKGSEVTA 231
                      :*   .* *:** * *.: :  :: :****::** :**  ::* .** *:  *::

1M17_A|SEQUENCE    ILEKGERLPQPPICTIDVYMIMVKCWMIDADSRPKFRELIIEFSKMARDPQRYLVIQGDE 296
1FPU_A|SEQUENCE    LLEKDYRMERPEGCPEKVYELMRACWQWNPSDRPSFAEIHQAFETMFQ------------ 276
1XBC_A|SEQUENCE    MLEKGERMGCPAGCPREMYDLMNLCWTYDVENRPGFAAVELRLRNYYY------------ 279
                   :***. *:  *  *. .:* :*  **  : ..** *  :   : .

1M17_A|SEQUENCE    RMHLPSPTDSNFYRALMDEEDMDDVVDADEYLIPQQG 333
1FPU_A|SEQUENCE    ------------------ESSISDEVEK--------- 286
1XBC_A|SEQUENCE    ----------------------DVVNEGHHHHHHHH 293
                                        * *:
```

Fig. 3. Multiple sequence alignment of EGFR (1 M17.pdb), SYK tyrosine kinase domain (1XBC.pdb), ABL kinase domain (1FPU.PDB). The alignment figure was created by ClustalW (1.83).

gives the main chain conformation as pairs of φ and ψ dihedral angles for each residue in the protein. The stereo-chemical parameters showed that more than 97% of the residues of all models had the (φ, ψ) dihedral angles in the most favored and the allowed regions of the Ramachandran plot as expected for a good model.

2.6. Binding site analysis

The binding site module [31] is a suite of programs in Insight II for identifying and characterizing protein active sites, binding sites, and functional residues from protein. This module was used to search for the protein active site and binding site by locating cavities in the protein structure. First, the protein was mapped onto a grid, which covers the complete protein space. The grid points were then defined as free points and protein points. The protein points were grid points, within 2 Å from a hydrogen atom or 2.5 Å from a heavy atom. The cubic eraser moves from the outside of the protein toward the center to remove the free points until the opening is too small for it to move forward. Those free points not reached by the eraser were defined as site points. The binding site can be used to guide the protein–ligand docking experiment.

2.7. Molecular 3D structure building (inhibitors/drugs considered for docking)

Inhibitors (**1**–**7**, Fig. 1) considered for docking were built by model builder in Cerius2 and minimized using conjugate gradient algorithm with a gradient convergence value of 0.01 kcal/mol Å. Partial atomic charges were calculated using the Gasteiger–Hückel method [32]. Further geometry optimization was carried out for each compound with the semi-empirical method using the AM1 Hamiltonian in MOPAC 6 in Cerius2 [33]. Initially, a constrained minimization for 100 cycles was performed in which 3 rings were defined as an aggregate to constrain their conformation to avoid false minima. The constraints were then removed, and the structure was subjected to 1000 cycles of minimization or till the gradient converged to 0.001 kcal/mol Å.

2.8. Molecular docking

Molecular docking can fit molecules together with a favorable configuration to form a complex system. The structural information from the theoretical modeled complex can help us to understand the catalytic mechanism of enzyme. The 3D structures of the new mutated EGFR structures were modeled with the 'Modeller' module. For tracking the interacting mode of EGFR and molecules, the advanced docking program "Affinity" was used to fulfill the automated molecular docking program (Accelrys Inc., San Diego, CA, USA).

The crystal structure of human, EGFR tyrosine kinase domain (1M17) with the inhibitor erlotinib, [6,7-bis (2-methoxy-ethoxy) quinazoline-4-yl]-(3-ethynylphenyl) amine [34] was obtained from Protein Data Bank (Fig. 4). H-atoms were added to the proteins while keeping all the residues in charged form. The best binding structure of the ligand to the receptor based on the energy of the ligand/receptor complex was automatically found by "Affinity", which uses a combination of Monte Carlo type and stimulated annealing procedure to dock a guest molecule to a host one. A key feature is that the bulk of the receptor, defined as the atoms, which is not in the binding site specified, holds rigid during the docking process, while the atoms in binding site and ligands are moveable.

The advantage of using 1M17 and 1XBC was only because it contains the inhibitor and hence subsequent docking studies could be easily performed using the model. The complex was subjected to minimization using steepest descent (1000 iterations) followed by conjugate gradient (1000 iterations) algorithms with CVFF force field. Implicit salvation parameters were considered. Amino acid residues in the region of 10 Å radius around the bound ligand were selected and allowed to be flexible while keeping rest of the protein rigid. These complexes were used as the starting conformation for further energy minimization and geometrical optimization before the final models were achieved.

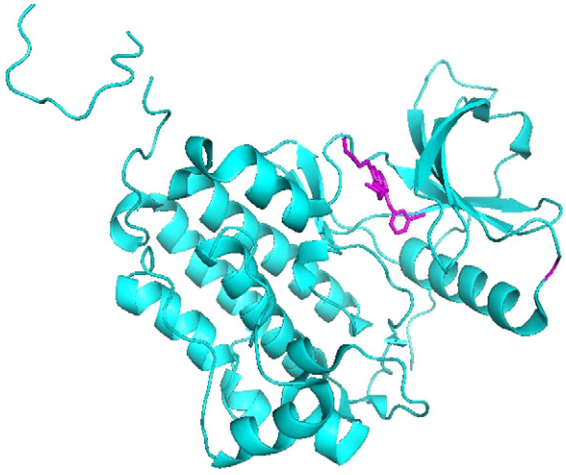

Fig. 4. The 3D structure of complex EGFR inhibitor-**1** M17.pdb (source: www.rcsb.org).

3. Results and discussion

3.1. Construction of mutated EGFR structure

Two new 3D structures of the EGFR with mutations at G695S and L834R were modeled using the 'Modeller' program using the crystal structure coordinates of SYK tyrosine kinase (1XBC.pdb) as templates as described above. This program is completely automated and is capable of generating energy minimized protein models by satisfying restraints on bond distances and dihedral angels. Each model was then subjected to various cycles of 'Modeller' and the best possible models were selected for further in silico studies. The resulting models were evaluated using the ENERGY command of Modeller and the program PROCHECK. Ramachandran plot statistics indicated that 91% of the main-chain dihedral angels were found in the most favorable region for G695S and 89% for L834R (Fig. 5a and b). The favorable region for WT EGFR was 90.81% (source: www.rcsb.org) These 3D structures of the homology built models were then superimposed on the experimental structure (1M17.pdb), and the root mean square deviation (RMSD) with respect to the Cα atoms were calculated and found to be 1.216 Å, 1.123 Å for G695S, L834R, respectively. In our study the RMSD values were in accordance with other changes in the three structures.

The models which were built as described above were used for active site docking of compounds, as in the EGFR crystal structure in which the orientation was towards erlotinib (conformer) which was visible in the structure; the same orientation was used for our affinity studies. The remaining compounds were then docked into the homology model and the resulting conformers were evaluated in the similarity analysis (based on grid interaction energies). These conformers are similar to the templates. This approach enables a conformer selection that constrains the conformational space to the active site of the homology model. The active site of

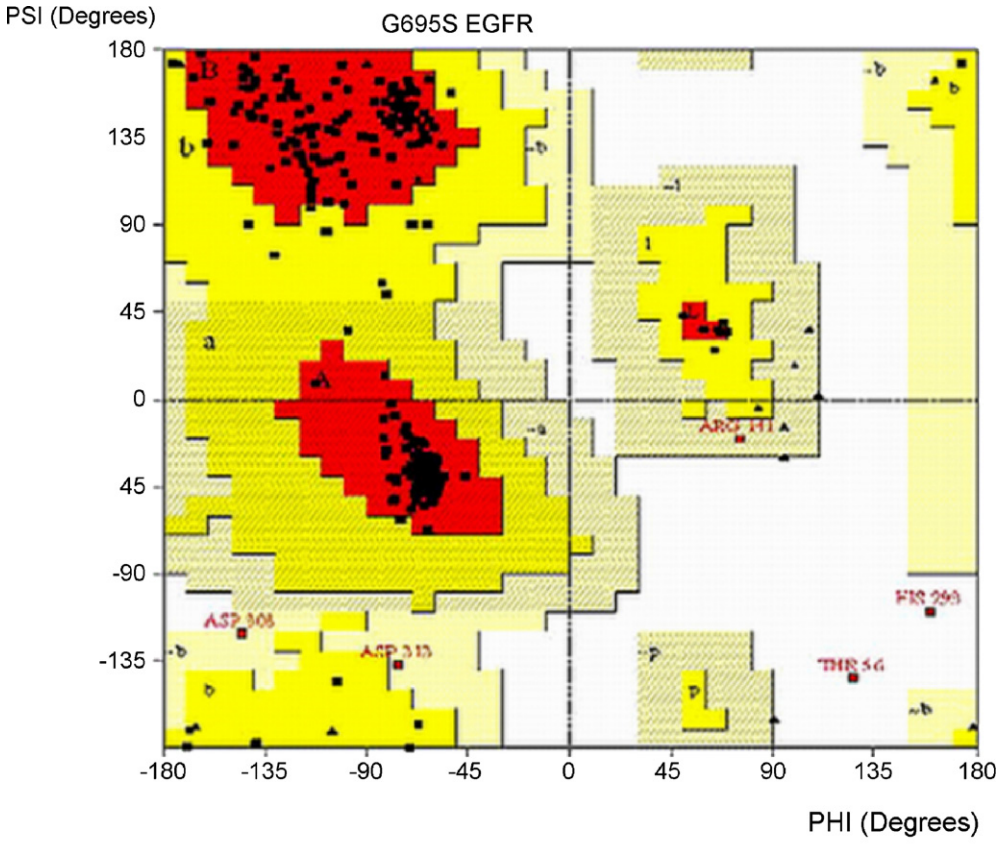

i.	Residues in most favored regions [A,B, L]	264	91.0%
ii.	Residues in additional allowed regions [a, b, l, p]	21	7.3%
iii.	Residues in generously allowed regions [~a, ~b, ~l, ~p]	2	1.0%
iv.	Residues in disallowed regions	3	0.0%
Number of non-glycine and non-proline residues		***290***	***100%***
i.	Number of end-residues (excl. Gly and Pro)	0	
ii.	Number of glycine residues (shown as triangles)	19	
iii.	Number of proline residues	18	
Total number of residues		***327***	

Fig. 5. (a) Ramachandran plot Produced by PROCHECK of the model build structure of **G695S** EGFR. (b) Ramachandran plot produced by PROCHECK of the model build structure of **L834R** EGFR.

the EGFR which has the mutations was analyzed and compared to EGFR crystal structure (1M17.pdb) with respect to structural differences. The surface area of mutant EGFR (G695S and L834R) and wild-type (WT) EGFR active sites as determined by Cerius 2 program was 657.73 Å.2/Unit.Cell, 753.76 Å.2/Unit.Cell, and 466.36 Å.2/Unit.Cell, respectively. The increase in surface area for the mutants could be due to the atomic chemistry with in the active site. The number of atoms in contact (within a distance of 4.5 Å) can be used to describe the local environment of a residue. As this number increases, the accessible surface area (ASA) of the residue decreases exponentially and each residue having its own set of parameters which also depend on whether the whole residue or just the side chain is considered. Hydrophobic and hydrophilic residues can be distinguished on the basis of both the average number of surrounding atoms and the variation of ASA.

3.2. Selection of ligands for docking

We have determined the response of seven quinazoline inhibitors such as gefitinib (**1**), erlotinib (**2**), CI-1033 (**3**), EKB-569 (**4**), and quinazoline analogues (**5**–**7**) (Fig. 1) [35,36]. Among all the seven inhibitors the first two (**1** and **2**) are already in the market, the inhibitors (CI-1033 and EKB-569) have entered clinical trials, whereas the other inhibitors (**5**–**7**) are only in the research stage.

These seven inhibitors are analogues of the parent compound quinazoline hence their properties vary only with the variations in the functional group of each compound. In our study their physiochemical properties implies their biological activities and binding affinities to the target.

EGFR belongs to the larger class of trans-membrane growth factor receptor tyrosine kinase (RTK). It consists of 1186 amino acid residues out of which the catalytic domain contains 333 residues. The mutations described above (G695S and L834R) are located in the GXGXXG motif of the nucleotide triphosphate binding domain or P-loop and adjacent to the highly conserved DFG motif in the activation loop. Both types of mutations showed the response to quinazoline inhibitors of EGFR. Using cheminformatics tools (Homology modeling and "Affinity") we tried to analyze these mutations with respect to gefitinib responses.

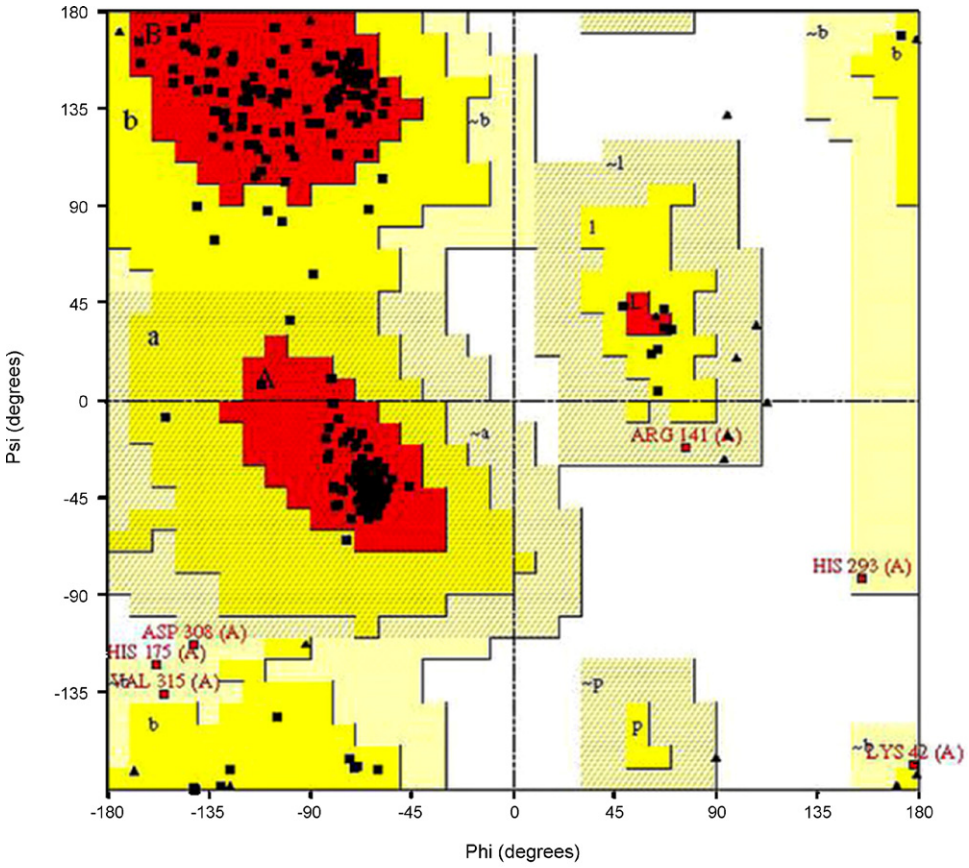

i.	Residues in most favored regions [A, B, L]	259	89.6%
ii.	Residues in additional allowed regions [a, b, l, p]	24	8.3%
iii.	Residues in generously allowed regions [~a, ~b, ~l, ~p]	6	2.1%
iv.	Residues in disallowed regions	0	0.0%
Number of non-glycine and non-proline residues		***289***	***100%***
i.	Number of end-residues (excl. Gly and Pro)	0	
ii.	Number of glycine residues (shown as triangles)	20	
iii.	Number of proline residues	18	
Total number of residues		***327***	

Fig. 5. (*Continued*).

3.3. Catalytic domain of the EGFR

The EGFR kinase domain adopts the bilobate-fold characteristics of all previously reported protein kinase domain. The N-terminal lobe (N-lobe) of the WT EGFR is formed mostly from beta strands and one helix, whereas the larger COOH terminal lobe (C-lobe) is mostly helical. The two lobes are separated by a cleft where ATP-competitive inhibitors have been found to bind. The important elements of the catalytic machinery bordering the cleft of the N-lobe include the glycine rich nucleotide phosphate-binding region (Gly695–Gly700). One of the apparently conservative changes in the glycine-rich loop of EGFR is with serine. Ser replaces the first Gly695 in the glycine-rich loop (Fig. 2). The serine substitution has an advantage, since it may interact with inhibitors due to its hydrophilic nature, and sensitivity between serine in the receptor towards the inhibitor. The serine mutation in the EGFR displays noticeable structural difference between the WT EGFR and the mutated EGFR structures.

In the WT EGFR the N1 and C8 edge of the quinazoline inhibitors were directed towards the N and C lobes of the peptide segments. The N1 of the quinazoline accepts an H-bond from the Met769 amide nitrogen. The other quinazoline nitrogen atom (N3) were not within H-bonding distance of the Thr766 side chain (4.1 Å), but a water molecule bridges this gap. Such a water molecule was observed by Shewchuk et al. in the P38/inhibitor complex [37]. The same water molecule contacts the side chain conformers. The less robust nature of this water mediated H-bonds between inhibitor EGFR parallels the relatively small effect on inhibitor affinity and it was seen as substitutions with carbon atom for N3 among compounds [38]. But in mutated models Met769 was within the hydrogen bond distance, so methionine may not form the bridge. This model showed higher affinity towards the receptors.

The second model of mutated EGFR had the leucine to arginine substitution at 834 positions in the A-loop of the catalytic domain. The arginine mutation at codon 834 may change the anti-parallel beta strand conformation in the A-loop. Underlying the central part of the A-loop, tyrosine 867 accepts an H-bond from arginine 834.

Normally many kinases have a homologous arginine (834) preceding the catalytic Asp (813) where it interacts with a highly conserved tyrosine. Tyr867 π-electrons interact with Arg834 in WT EGFR. It is therefore predicted that in the Arg834 mutation may be involved in the interactions with the OH group of Tyr867 because of the smaller distance between the two molecules. This may also show a favorable higher catalytic activity with the inhibitor. The presence of four glutamate residues (841, 842, 844, and 848) in the catalytic domain of EGFR is suggestive of its intrinsic catalytic activity. The EGFRK A-loop is rich in glutamate residues, and the contribution of two of these residues (Glu842 and Glu844) to EGFRK function was demonstrated using amino acid substitutions that altered the in vitro kinetics of phospho-transfer. Since the unphosphorylated A-loop in EGFRK incompatible with substrate binding and gets blocked at ATP binding site due to unphosphorylation at insulin receptor kinase (IRK) as well as tyrosine sites, many energetically beneficial interactions stabilize this conformation. A H-bond between side chain of tyrosine and glutamate (8 4 8) mimics that between tyrosine and the main chains nitrogen of glycine in p-IRK, but the electron density supporting the glutamate side chain conformation is weak. This relationship between these chemistries is contained to the catalytic activity machinery and substrate for phospho-transfer. The hydrophobicity of this region therefore has demonstrated attractions towards the inhibitors. L834R also increases the hydrophobicity in the A-loop; this is due to the guanidine group present in the amino acid (Arg). Therefore, it may be possible that L834R mutations render the receptor more amenable to quinazoline inhibitors. From this study it is concluded that both mutations G695S and L834R in the EGFR are expected to exert good response to the quinazoline inhibitors.

3.4. Energy calculations for all inhibitors used for docking

The interaction energy of the quinazoline inhibitors with each individual amino acid in the active site of EGFR was calculated by the advanced program "Affinity". Residues LEU_A694/23 (crystal structure residue number/homology model residue number), GLY_A695/24, VAL_A702/31, ALA_A719/48, LEU_A764/93, THR_A766/95, GLN_A767/96, LEU_A768/97, MET_A769/98, GLY_A772/101, THR_A830/159, ASP_A831/160, GLY_A833/162 were seen to have significant interactions with the inhibitor and important for binding (Fig. 6). It was interesting to observe that the inhibitors in the mutated EGFR G695S did not interact with MET_A742/71. Also, in the EGFR crystal structure (wild-type) LEU_834/163 did not interact with the inhibitors. The overall binding affinity of the molecule was slightly affected, but surprisingly the mutated serine residue was found to have better interaction with the inhibitor molecule except erlotinib. EGFR WT (crystal structure) interaction energies, i.e. the total energy (E_{total}) values (electrostatic and steric) were −0.161 kcal/mol (CI-1033), −0.877 kcal/mol (gefitinib), −0.951 kcal/mol (erlotinib), and the total energy values for EGFR mutated Ser24 were −1.314 kcal/mol (CI-1033), −1.504 kcal/mol (gefitinib), −0.786 kcal/mol (erlotinib). In crystal structure Leu834 did not interact with the inhibitors but in the arginine mutation it was found to interact with inhibitors and gave good affinity. So gefitinib and CI-1033 exhibited good sensitivity in the mutated EGFR.

3.5. Evaluation of the amino acid residues in the binding site of EGFR

The active site of EGFR comprising 15 amino acid residues were also evaluated for interactions with the seven inhibitors in this study. The consolidated interactions of each inhibitor with the EGFR receptors (wild-type and two mutated types G695S and L834R) are presented in Table 1. The non-bonded interactions, Van der Waals and Coulomb interactions were evaluated for each protein and plotted in graphs (Graphs 1–3). We found that the L834R and G695S mutations in EGFR possibly disrupt inhibitory interactions within the EGFR. Structural examination of the inhibitor complexes revealed that the mutations can affect the way the inhibitors interact with the enzyme. Interestingly, the inhibitors-**1**, -**4**, -**5**, and -**6** bind more tightly to the L834R mutated model than to the wild-type EGFR.

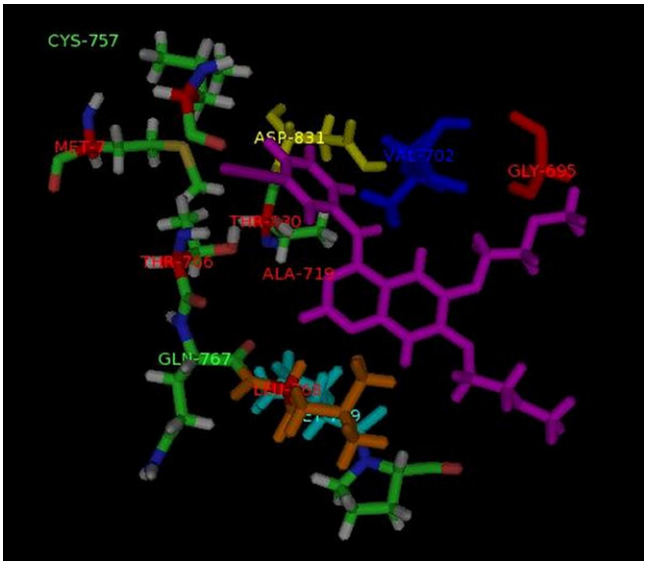

Fig. 6. Catalytic amino acid residues as depicted in Table 1 (15 amino acids) are shown in different colors in this figure around the inhibitor molecule which is in magenta color in the central part of the figure. This figure represents the amino acids of the model in the close vicinity of the inhibitor.

3.6. Calculations of the distance between side chain atoms and the inhibitors

Further investigations were carried out by measuring the distances in the receptor–inhibitor complexes for all the seven inhibitors that predicted the type of interactions on mutated points. The distances in angstroms between the side chain atom of each inhibitor and the Gly695 in WT EGFR (Table 2) and G695S in the mutated EGFR (Table 3) were measured for possible interactions. These results are presented in the tables (Tables 2 and 3) after visualizing receptor–inhibitor complexes. WT EGFR interactions were taken as reference for comparing the distance between the inhibitor and receptor in mutated EGFR models.

Here we describe the interactions of the inhibitors with the two mutated models as compared to the wild-type EGFR. In the first model substitution for Leu834 to arginine in EGFR brings about changes in interactions with other amino acids such as Gln_A767/96 for inhibitors-**4**, -**5**, and -**7**. Other inhibitors weakly interacted with Gln_A767/96 amino acid residue. These inhibitors exhibited Van der Waals interactions with the mutated residue Leu_834/Arg_163, compared to WT-EGFR receptor. This proves that the mutations in EGFR (L834R) could attract the ligands (Table 1). In Table 1 we have demonstrated the interactions of active site amino acids, which release the free energy at the time of complex formation. Hence the observations of these highly interactive amino acids are compared for the cumulative effect of each inhibitor.

In the second model, serine substitution for Gly695 in EGFR receptor enhanced the Van der Waals interactions, even though the electrostatic interactions were found to be nil. In the L834R

Table 1
The total energy (E_{total}), Vanderwaals energy (E_{vdw}), and electrostatic energy (E_{ele}) between inhibitors-**1**–**7** and individual residues

Residue	EGFR WT activity			Mutated EGFR activity[a] (G695S)			Mutated EGFR activity[a] (L834R)		
	E_{ele}	E_{vdw}	E_{total}	E_{ele}	E_{vdw}	E_{total}	E_{ele}	E_{vdw}	E_{total}
Inhibitor-**1**									
LEU_A694/23	−0.035	−3.643	−3.677	−0.25	−2.438	−2.688	−0.337	−2.593	−2.93
GLY_A695/24[b]	0.184	−1.061	−0.877	−0.193	−1.311	−1.504	−1.371	−1.288	−2.659
VAL_A702/31	−0.132	−2.165	−2.297	−0.045	−2.357	−2.402	0.059	−2.444	−2.385
ALA_A719/48	0.131	−1.002	−0.871	0.033	−0.854	−0.82	−0.012	−1.065	−1.077
MET_A742/71	−0.093	−0.478	−0.571	–[c]	–[c]	–[c]	−0.068	−0.348	−0.415
LEU_A764/93	0.014	−0.599	−0.585	0.02	−0.5	−0.48	−0.061	−0.872	−0.933
THR_A766/95	−0.376	−0.945	−1.324	−0.004	−1.177	−1.181	0.124	−1.402	−1.278
GLN_A767/96	−0.28	−0.574	−0.853	−0.335	−0.637	−0.972	−0.373	−0.198	−0.571
LEU_A768/97	−0.013	−1.591	−1.604	−0.18	−2.056	−2.236	−0.189	−2.061	−2.25
MET_A769/98	−0.593	−1.936	−2.529	−0.193	−1.506	−1.699	−0.734	−2.07	−2.804
GLY_A772/101	−0.469	−1.415	−1.883	−0.556	−1.077	−1.633	−0.054	−1.25	−1.304
THR_A830/159	−0.171	−1.36	−1.531	−0.055	−1.553	−1.608	0.236	−1.8	−1.564
ASP_A831/160	0.12	−1.247	−1.128	−0.126	−1.306	−1.432	−3.524	−0.82	−4.344
GLY_A833/162	0.017	−0.025	−0.008	−0.009	−0.014	−0.023	−0.006	−0.018	−0.024
LEU_834/163[b]	–[c]	–[c]	–[c]	−0.051	−0.343	−0.394	0.407	−0.651	−0.224
Inhibitor-**2**									
LEU_A694/23	−0.458	−3.166	−3.624	−0.728	−3.448	−4.176	−0.367	−3.253	−3.62
GLY_A695/24[b]	−0.139	−0.812	−0.951	0.176	−0.962	−0.786	−0.051	−0.664	−0.716
VAL_A702/31	−0.201	−2.192	−2.393	−0.048	−2.719	−2.767	−0.191	−1.982	−2.173
ALA_A719/48	−0.293	−1.22	−1.513	−0.269	−1.008	−1.277	−0.136	−0.857	−0.993
MET_A742/71	−0.074	−0.62	−0.693	–[c]	–[c]	–[c]	0.02	−0.358	−0.338
LEU_A764/93	0.001	−0.54	−0.54	0.281	−0.915	−0.634	0.483	−0.903	−0.42
THR_A766/95	−0.428	−1.322	−1.75	−0.229	−1.272	−1.501	−0.543	−1.776	−2.318
GLN_A767/96	−0.225	−0.536	−0.761	−0.225	−0.622	−0.847	−0.305	−0.379	−0.684
LEU_A768/97	−0.12	−1.759	−1.879	−0.13	−2.063	−2.193	−0.29	−2.085	−2.375
MET_A769/98	−0.478	−2.017	−2.495	−0.191	−1.589	−1.78	−0.604	−1.871	−2.474
GLY_A772/101	−0.628	−1.661	−2.289	−0.949	−1.794	−2.744	−1.221	−1.62	−2.841
THR_A830/159	−0.535	−1.675	−2.21	−0.125	−1.589	−1.714	−0.23	−2.078	−2.308
ASP_A831/160	0.151	−1.51	−1.36	−0.21	−1.152	−1.361	−1.286	−0.463	−1.748
GLY_A833/162	0.018	−0.027	−0.009	0.004	−0.013	−0.009	0.002	−0.018	−0.017
LEU_834/163[b]	–[c]	–[c]	–[c]	0.019	−0.388	−0.369	0.095	−0.523	−0.428
Inhibitor-**3**									
LEU_A694/23	0.132	−0.348	−0.216	0.3	−3.527	−3.226	0.55	−4.044	−3.493
GLY_A695/24[b]	0.066	−0.227	−0.161	0	−1.312	−1.314	−0.286	−1.123	−1.409
VAL_A702/31	0.998	29.617	30.616	0.071	−2.973	−2.902	0.027	−1.909	−1.881
ALA_A719/48	0.335	−0.409	−0.073	0.178	−0.891	−0.713	0.268	−0.81	−0.542
MET_A742/71	−0.144	0.056	−0.088	–[c]	−2	−2	−0.044	−0.161	−0.204
LEU_A764/93	0.078	−0.497	−0.419	0.004	−0.696	−0.691	0.033	−0.775	−0.741
THR_A766/95	−0.223	2.87	2.646	−0.011	−0.894	−0.905	−0.009	−1.058	−1.067
GLN_A767/96	−0.391	−0.306	−0.696	−0.382	−0.621	−1.003	−0.33	−0.547	−0.877
LEU_A768/97	0.225	−1.478	−1.253	0.028	−1.882	−1.854	0.01	−1.774	−1.765
MET_A769/98	−0.641	−0.57	−1.211	−0.345	−1.657	−2.002	−0.561	−1.753	−2.314
GLY_A772/101	−0.132	−0.247	−0.379	−0.05	−0.726	−0.775	0.196	−1.436	−1.239
THR_A830/159	0.063	−0.044	0.02	−0.011	−1.611	−1.622	0.374	−1.646	−1.272
ASP_A831/160	0.043	−0.056	−0.013	0.114	−1.503	−1.39	−3.348	−0.477	−3.824
GLY_A833/162	0.035	−0.009	0.026	−0.005	−0.015	−0.02	−0.005	−0.012	−0.017
LEU_834/163[b]	−2	−2	−2	−0.007	−0.107	−0.507	0.232	−0.372	−0.14
Inhibitor-**4**									
LEU_A694/23	−0.431	−2.621	−3.052	−0.479	−3.56	−4.038	−0.164	−2.589	−2.753
GLY_A695/24[b]	−0.561	−0.817	−1.378	−0.071	−1.511	−1.582	−0.184	−0.441	−0.625
VAL_A702/31	−0.127	−2.332	−2.459	−0.187	−2.667	−2.854	0.202	−2.989	−2.788
ALA_A719/48	0.234	−1.483	−1.249	0.227	−1.021	−0.794	0.127	−2.015	−1.888
MET_A742/71	−0.176	−0.796	−0.972	–[c]	–[c]	–[c]	0.039	−0.438	−0.477
LEU_A764/93	−0.064	−0.682	−0.746	0.127	−0.17	−0.043	−0.181	−1.068	−1.249
THR_A766/95	−0.876	−1.395	−2.271	−0.168	−0.721	−0.889	−0.04	−0.725	−0.765
GLN_A767/96	−0.491	−0.669	−1.16	0.292	−0.59	−0.299	−0.516	−0.414	−0.93
LEU_A768/97	0.012	−1.823	−1.811	0.403	−1.232	−0.828	−0.118	−2.048	−2.166
MET_A769/98	−0.967	−2.158	−3.125	0.143	−1.785	−1.642	−0.832	−2.502	−3.334
GLY_A772/101	0.101	−1.308	−1.207	−0.048	−1.885	−1.934	0.297	−0.803	−0.505
THR_A830/159	−0.521	−1.665	−2.187	−0.01	−1.379	−1.389	0.79	−2.127	−1.337
ASP_A831/160	0.082	−1.797	−1.715	0.272	−1.192	−0.92	−5.558	−1.526	−7.084
GLY_A833/162	0.026	−0.033	−0.007	−0.003	−0.008	−0.011	−0.005	−0.022	−0.027
LEU_834/163[b]	–[c]	–[c]	–[c]	−0.107	−0.211	−0.318	0.559	−0.787	−0.228
Inhibitor-**5**									
LEU_A694/23	−0.241	−3.868	−4.109	−0.541	−3.007	−3.548	−0.087	−0.814	−0.902
GLY_A695/24[b]	0.159	−0.399	−0.241	−0.027	−1.416	−1.444	0.117	−0.247	−0.13
VAL_A702/31	0.018	−2.285	−2.268	−0.003	−2.644	−2.648	0.026	−1.95	−1.924
ALA_A719/48	0.239	−1.613	−1.375	0.348	−1.436	−1.088	0.009	−2.314	−2.305
MET_A742/71	−0.185	−0.606	−0.791	–[c]	–[c]	–[c]	−0.09	−0.301	−0.39

Table 1 (*Continued*)

Residue	EGFR WT activity			Mutated EGFR activity[a] (G695S)			Mutated EGFR activity[a] (L834R)		
	E_{ele}	E_{vdw}	E_{total}	E_{ele}	E_{vdw}	E_{total}	E_{ele}	E_{vdw}	E_{total}
LEU_A764/93	−0.038	−0.877	−0.914	0.091	−0.503	−0.412	−0.166	−0.918	−1.084
THR_A766/95	−0.338	−1.69	−2.028	−0.183	−0.38	−0.563	−0.17	0.096	−0.074
GLN_A767/96	−0.532	−0.564	−1.096	−0.022	−0.795	−0.816	−0.175	−0.853	−1.028
LEU_A768/97	−0.1	−2.042	−2.142	0.279	−1.551	−1.272	−0.204	−2.65	−2.853
MET_A769/98	−0.982	−2.04	−3.022	0.009	−1.781	−1.772	−1.196	−1.479	−2.675
GLY_A772/101	0.02	−1.62	−1.6	−0.047	−1.529	−1.576	−0.362	−1.854	−2.217
THR_A830/159	−0.726	−1.719	−2.445	0.139	−1.623	−1.485	0.698	−1.359	−0.661
ASP_A831/160	0.094	−1.575	−1.48	0.172	−1.204	−1.032	−2.228	−0.799	−3.027
GLY_A833/162	0.029	−0.032	−0.003	−0.008	−0.013	−0.02	−0.006	−0.017	−0.023
Inhibitor-**6**									
LEU_A694/23	−0.581	−3.79	−4.371	−0.044	−2.977	−3.021	−0.353	−3.268	−3.62
GLY_A695/24[b]	0.389	−0.672	−0.282	−0.076	−0.767	−0.843	0.01	−0.621	−0.611
VAL_A702/31	−0.139	−2.49	−2.629	−0.322	−3.209	−3.531	−0.104	−2.516	−2.62
ALA_A719/48	−0.192	−1.789	−1.982	−0.002	−1.453	−1.456	0.223	−1.736	−1.513
MET_A742/71	−0.138	−0.781	−0.919	–[c]	–[c]	–[c]	0.034	−0.282	−0.248
LEU_A764/93	−0.071	−0.423	−0.494	0.263	−0.883	−0.620	0.205	−0.852	−0.647
THR_A766/95	−0.914	−1.278	−2.193	−0.398	−0.994	−1.391	−0.668	−0.603	−1.271
GLN_A767/96	−0.162	−0.917	−1.079	−0.093	−0.928	−1.021	−0.17	−0.961	−1.131
LEU_A768/97	−0.061	−1.757	−1.818	−0.089	−1.794	−1.883	−0.028	−1.738	−1.766
MET_A769/98	−0.346	−2.069	−2.416	0.569	−1.754	−1.185	0.235	−1.684	−1.449
GLY_A772/101	−0.38	−1.69	−2.07	−1.167	−1.626	−2.793	−0.323	−1.705	−2.028
THR_A830/159	−0.771	−1.827	−2.598	−0.045	−1.912	−1.957	0.23	−2.123	−1.894
ASP_A831/160	0.407	−1.908	−1.502	0.095	−1.196	−1.101	−2.086	−0.842	−2.928
GLY_A833/162	0.043	−0.03	0.013	0.003	−0.015	−0.012	0.002	−0.017	−0.015
LEU_834/163[b]	–[c]	–[c]	–[c]	0.016	−0.374	−0.358	0.124	−0.492	−0.368
Inhibitor-**7**									
LEU_A694/23	−0.391	−3.456	−3.847	0.027	−0.68	−0.653	−0.516	−3.246	−3.762
GLY_A695/24[b]	−0.054	−0.99	−1.044	0.232	−0.83	0.598	−0.013	−0.58	−0.594
VAL_A702/31	−0.162	−2.352	−2.515	−0.176	−1.93	−2.106	−0.237	−2.212	−2.449
ALA_A719/48	0.361	−1.511	−1.151	0.461	−0.203	−0.461	0.501	−1.568	−1.068
MET_A742/71	−0.163	−0.683	−0.846	–[c]	–[c]	–[c]	−0.055	−0.14	−0.195
LEU_A764/93	−0.041	−0.915	−0.956	−0.153	−0.458	0.611	0.048	−0.772	−0.724
THR_A766/95	−1.304	−1.207	−2.51	−0.59	−0.934	−1.524	−0.235	−0.414	−0.649
GLN_A767/96	−0.313	−0.79	−1.103	−0.408	−1.917	−2.35	−0.205	−0.847	−1.051
LEU_A768/97	0.119	−1.811	−1.692	0.76	−1.386	−0.626	0.118	−2.134	−2.016
MET_A769/98	−0.725	−2.131	−2.856	0.191	−1.288	−1.097	−0.593	−1.792	−2.384
GLY_A772/101	−0.303	−1.985	−2.288	−1.126	−0.577	−1.703	−0.791	−2.066	−2.857
THR_A830/159	−0.528	−1.619	−2.148	0.308	−1.498	2.086	0.37	−1.658	−1.288
ASP_A831/160	0.003	−1.663	−1.66	0.075	−0.027	0.048	−1.391	−0.35	−1.74
GLY_A833/162	0.008	−0.027	−0.019	0.065	−0.017	0.048	−0.004	−0.011	−0.015
LEU_834/163[b]	–[c]	–[c]	–[c]	−0.006	−0.143	0.149	0.202	−0.294	−0.092

[a] Values were measured in kcal/mol.
[b] Indicates mutated amino acids.
[c] No interaction with that amino acid and inhibitor.

mutated EGFR receptor, Gly695 was found to be more interactive with the inhibitors-**1**, -**3**, and -**6** and less interactive with inhibitors-**2**, -**4**, -**5**, and -**7** with respect to total interactions. The functional groups as mentioned in (Table 3) have shown promising interactions with mutated points on the receptor. Inhibitor-**2** had better affinity with respect to the distance between the inhibitor and the receptor (Tables 2 and 3).

Table 2
Distance in angstroms between the side chain atom of each inhibitor and the Gly695 in WT EGFR

Inhibitor	Inhibitor position	A.A position	Distance (Å)
Inhibitor-**1**	CH_2	N–H	5.21
Inhibitor-**2**	CH_2	N–H	4.21
Inhibitor-**2**	C═O	H_2C–NH_2	3.41
Inhibitor-**3**	CH═CH	N–H	4.04
Inhibitor-**3**	C═O	H_2C–NH_2	2.76
Inhibitor-**4**	CH_2	N–H	3.36
Inhibitor-**4**	Aryl–O	H_2C–NH_2	4.78
Inhibitor-**5**	O–CH_2	N–H	3.50
Inhibitor-**5**	CH_2–O	H_2C–NH_2	4.42
Inhibitor-**6**	O–CH_2–CH_2	N–H	3.70
Inhibitor-**6**	Aryl-O	H_2C–NH_2	4.42
Inhibitor-**7**	CH_3	N–H	3.65
Inhibitor-**7**	CH_3–O	H_2C–NH_2	3.20

3.7. Receptor and inhibitor interactions

The active site of the EGFR consisting of 15 amino acid residues were identified in the wild-type EGFR and the two mutated models G695S and L834R, and these were evaluated to determine the forces of attractions between the ligands and the receptor sites. Using the "Affinity" package of Accelrys, we were able to calculate the energy data for each inhibitor individually and comparatively between the three models of EGFR (WT, G695S, and L834R). This data has been presented in Table 1. It is clearly seen from this data that we could identify the variations of attractions between each inhibitor towards the three models tested. The data generated using the seven inhibitors with wild-type EGFR, and two mutated EGFRs (G695S and L834R) which were constructed in this study showed that

Inhibitor-**1**: Gefitinib had low total energy indicating high affinity towards the mutated G695S-EGFR, L834R-EGFR structures. The motif 4-fluoro-3-chlorophenyl present in gefitinib emerged as a preferred group to confer metabolic stability and thus enhanced

Table 3
Distance in angstroms between the side chain atom of each inhibitor and the Ser24 in mutated EGFR (G695S)

Inhibitor	Inhibitor position	A.A position	Distance (Å)
Inhibitor-**1**	CH_2–CH_2	N–H	4.07
Inhibitor-**1**	Aryl	OH–CH_2–CH_2	3.63
Inhibitor-**3**	CH_2–CH_2–CH_2	N–H	5.21
Inhibitor-**3**	CH_2–N	OH–CH_2–CH_2	3.53
Inhibitor-**3**	C═C–C═O	CH_2–OH	3.26
Inhibitor-**4**	CH_2–CH_2	N–H	4.33
Inhibitor-**4**	Aryl	OH–CH_2–CH_2	3.23
Inhibitor-**5**	O–CH_2–CH_2	N–H	3.52
Inhibitor-**5**	CH_3–O–CH_2	OH–CH_2–CH_2	3.42
Inhibitor-**5**	CH_3–O	CH_2–OH	3.82
Inhibitor-**6**	CH_2–CH_2–CH_2	N–H	4.28
Inhibitor-**6**	Aryl	OH–CH_2–CH_2	4.28
Inhibitor-**7**	CH_2–CH_2	N–H	4.37
Inhibitor-**7**	CH_3–O–CH_2	OH–CH_2–CH_2	3.21
Inhibitor-**7**	CH_3–O	CH–OH	3.05

in vivo activity. The docking experiments seem to indicate that the chlorine and fluorine atoms at the phenyl group were in Van der Waals contact with Ser695. It also showed shorter distance in the docking studies with the G695S EGFR structure compared to wild-type receptor. This finding explains the observation that tumors bearing this mutation have been found to be more responsive to treatment with gefitinib.

Inhibitor-**2**: the interplanar angle of aromatic ring systems in erlotinib is 42°. This directs the acetylene moiety into a binding pocket. Erlotinib is found in the cleft between amino-terminal and carboxy-terminal lobes. Erlotinib lies with the N1- and C8-containing edge of the quinazoline directed toward the peptide segment connecting N- and C-lobes, with the ether linkages projecting past the connecting segment into solvent and the anilino substituent on the opposite end sequestered in a hydrophobic pocket. This hydrophobicity of the pocket was changing due to mutated amino acids of arginine and serine. But it was found that the inhibitor did not interact with the Met742 in G695S EGFR structure, maybe this is also one of the reasons for showing less affinity. Erlotinib showed high total energy indicating low affinity towards the G695S EGFR structure compared to wild-type EGFR. Therefore this ligand may prove to be useful for those patients who do not have mutations in the EGFR, as determined in the docking studies.

Inhibitor-**3**: inhibitor CI-1033 showed good affinity towards the G695S EGFR structure, as compared to either the wild-type EGFR or the L834R EGFR structure. The 4-(4-fluoro-3-chloroanilino) substituent is adjacent to Cys751 and Met742 and can form favorable sulfur–aromatic interactions. The fact that there are very limited sites for favorable substitution of the 4-(4-fluoro-3-chloroanilino) ring is in agreement with the restricted size of this pocket. The additional binding energy provided by the 4-(4-fluoro-3-chloroanilino) substitution in this deep pocket may be the reason for the extremely high binding affinity of this inhibitor. As shown in Table 1, we found strong VDW repulsions between VAL-A702 for the inhibitor-**3** for the WT. This is due to the alkanes in the valine structure which forms the eclipsing hydrogen with the inhibitor.

Inhibitor-**4**: EKB-569 inhibitor showed good affinity towards the L834R EGFR structure as compared to the G695S EGFR and the WT EGFR. EKB-569 compound is designed to block kinase activity by binding to the ATP site of the enzyme. This compound is structurally similar to reversible anilinoquinazoline inhibitors such as gefitinib, but contains a reactive Michael-acceptor that forms a covalent bond with Cys797 at the edge of the ATP cleft. Actually this compound relies on displacement of the bridging water molecule. On the C3 position bears a cyano group that projects its nitrogen towards Thr766. The reduction between the two molecules allows a direct hydrogen bond thus eliminating the need for a water bridge. The decrease in binding affinity resulting from the proposed hydrogen bonding opportunity; however it is also possible that unfavorable repulsive electrostatic interactions with the 8-aza compound. Or steric hindrance upon alkyl substitution with the peptide backbone might also play a role. The distance between the aryl group of the inhibitor and the serine functional group was larger in the G695S EGFR and WT EGFR compared to L834R EGFR, even though it has shown less distance from aryl group of the inhibitor.

Inhibitors-**5**–**7**: among these three inhibitors only the seventh inhibitor showed lower affinity towards the L834R EGFR, whereas the other inhibitors-**5** and -**6** showed a better response compared to WT EGFR. The distance between the receptor and the inhibitors-**5** and -**6**, was much smaller compared to the distance between inhibitor-**7** and the receptor. All these results indicate that total energy was inversely proportional to the affinity. This study on distances predicts the conformational changes in the internal structure of the active site.

4. Conclusions

In this study we have predicted the affinity of seven individual inhibitors to the two new modeled EGF receptors and compared their affinity towards the wild-type EGFR. The data which is presented in Table 1 shows the affinity and total energy values for each inhibitor generated using in silico studies. The interactions of the inhibitors which were docked to the ATP domains of the EGFR structures have been evaluated and the distances between the nearest (EGFR) amino acid and ligand molecules was measured and tabulated and all the total energy values were calculated to determine the stability of the receptor ligand complex for each set of experiments. Inhibitors designed specifically to target mutants such as L834R and G695S should, in principle, be less toxic due to reduced inhibition of the wild-type kinase. This may help to guide rational use of currently available EGFR inhibitors and provides new direction for the design and development of even more potent inhibitors that are tailored to specific EGFR mutants.

Appendix A. Supplementary data

Supplementary data associated with this article can be found, in the online version, at doi:10.1016/j.jmgm.2008.04.010.

References

[1] I. Alroy, Y. Yarden, The ErbB signaling network in embryogenesis and oncogenesis: signal diversification through combinatorial ligand–receptor interactions, FEBS Lett. 410 (1997) 83–86.
[2] P. Yaish, A. Gazit, C. Gilon, A. Levitzki, Blocking of EGF dependent cell proliferation by EGF receptor kinase inhibitors, Science 242 (1988) 933–935.
[3] A. Levitzki, Protein tyrosine kinase inhibitors as novel therapeutic agents, Pharmacol. Ther. 82 (1999) 231–239.
[4] Y. Yarden, The EGFR family and its ligands in human cancer. Signalling mechanisms and therapeutic opportunities, Eur. J. Cancer 37 (2001) S3–8S.
[5] J. Baselga, Why the epidermal growth factor receptor? The rationale for cancer therapy, Oncologist 7 (2002) 2–8.
[6] K. Khazaie, V. Schirrmacher, R.B. Lichtner, EGF receptor in neoplasia and metastasis, Cancer Metastasis Rev. 12 (1993) 255–274.
[7] M.W. Pedersen, H.S. Poulsen, Epidermal growth factor receptor in cancer therapy, Sci. Med. 8 (2002) 206–217.
[8] J.G. Paez, P.A. Janne, J.C. Lee, S. Tracy, H. Greulich, S. Gabriel, P. Herman, F.J. Kaye, N. Lindeman, T.J. Boggon, K. Naoki, H. Sasaki, Y. Fujii, M.J. Eck, W.R. Sellers, B.E. Johnson, M. Meyerson, EGFR mutations in lung cancer: correlation with clinical response to gefitinib therapy, Science 304 (2004) 1497–1500.
[9] M. Ono, A. Hirata, T. Kometani, M. Miyagawa, S. Ueda, H. Kinoshita, T. Fujii, M. Kuwano, Sensitivity to gefitinib (Iressa, ZD1839) in non-small cell lung cancer cell lines correlates with dependence on the epidermal growth factor (EGF) receptor/extracellular signal-regulated kinase 1/2 and EGF receptor/Akt pathway for proliferation, Mol. Cancer Ther. 3 (2004) 465–472.

[10] H. Greulich, T.H. Chen, W. Feng, P.A. Janne, J.V. Alvarez, M. Zappaterra, S.E. Bulmer, D.A. Frank, W.C. Hahn, W.R. Sellers, M. Meyerson, Oncogenic transformation by inhibitor-sensitive and -resistant EGFR mutants, PLoS Med. 2 (2005) e313.
[11] S. Kobayashi, T.J. Boggon, T. Dayaram, P.A. Janne, O. Kocher, M. Meyerson, B.E. Johnson, M.J. Eck, D.G. Tenen, B. Halmos, EGFR mutation and resistance of non-small-cell lung cancer to gefitinib, N. Engl. J. Med. 352 (2005) 786–792.
[12] H. Assefa, S. Kamath, J.K. Buolamwini, 3D-QSAR and docking studies on 4-anilinoquinazoline and 4-anilinoquinoline epidermal growth factor receptor (EGFR) tyrosine kinase inhibitors, J. Comput. Aid. Mol. Des. 17 (2003) 475–493.
[13] P. Traxler, N. Lydon, Recent advances in protein tyrosine kinase inhibitors, Drugs Fut. 20 (1995) 1261–1274.
[14] P. Traxler, P. Furet, Strategies toward the design of novel and selective protein tyrosine kinase inhibitors, Pharmacol. Ther. 82 (1999) 195–206.
[15] M.J. Morin, From oncogene to drug: development of small molecule tyrosine kinase inhibitors as anti-tumor and anti-angiogenic agents, Oncogene 19 (2000) 6574–6583.
[16] P. Cohen, Protein kinases—the major drug targets of the twenty-first century? Nat. Rev. Drug Discov. 1 (2002) 309–315.
[17] S.R. Hubbard, Protein tyrosine kinases: autoregulation and small-molecule inhibition, Curr. Opin. Struct. Biol. 12 (2002) 735–741.
[18] J. Dancey, E.A. Sausville, Issues and progress with protein kinase inhibitors for cancer treatment, Nat. Rev. Drug Discov. 2 (2003) 296–313.
[19] International conference on bioinformatics of genome regulation and structure. Novosibirsk, Russia, 2006.
[20] INSIGHT II Molecular Modelling Package, Accelrys, San Diego, MSI, USA, 1997.
[21] A. Bairoch, R. Apweiler, The SWISS-PROT protein sequence database and its supplement TrEMBL in 2000, Nucleic Acids Res. 28 (2000) 45–48.
[22] S.F. Altschul, T.L. Madden, A.A. Schaffer, J. Zhang, Z. Zhang, W. Miller, D.J. Lipman, Gapped BLAST and PSI-BLAST: a new generation of protein database search programs, Nucleic Acids Res. 25 (1997) 3389–3402.
[23] S. Atwell, J.M. Adams, J. Badger, M.D. Buchanan, I.K. Feil, K.J. Froning, X. Gao, J. Hendle, K. Keegan, B.C. Leon, H.J. Muller-Dieckmann, V.L. Nienaber, B.W. Noland, K. Post, K.R. Rajashankar, A. Ramos, M. Russell, S.K. Burley, S.G. Buchanan, A novel mode of Gleevec binding is revealed by the structure of spleen tyrosine kinase, J. Biol. Chem. 279 (2004) 55827–55832.
[24] T. Schindler, W. Bornmann, P. Pellicena, W.T. Miller, B. Clarkson, J. Kuriyan, Structural mechanism for STI-571 inhibition of abelson tyrosine kinase, Science 289 (2000) 1938–1942.
[25] H. Yamaguchi, W.A. Hendrickson, Structural basis for activation of human lymphocyte kinase Lck upon tyrosine phosphorylation, Nature 384 (1996) 484–489.
[26] S.R. Hubbard, L. Wei, L. Ellis, W.A. Hendrickson, Crystal structure of the tyrosine kinase domain of the human insulin receptor, Nature 372 (1994) 746–754.
[27] J.D. Thompson, D.G. Higgins, T.J. Gibson, CLUSTAL W: improving the sensitivity of progressive multiple sequence alignment through sequence weighting, position-specific gap penalties and weight matrix choice, Nucleic Acids Res. 22 (1994) 4673–4680.
[28] A. Sali, T.L. Blundell, Comparative protein modelling by satisfaction of spatial restraints, J. Mol. Biol. 234 (1993) 779–815.
[29] M.A. Marti-Renom, A.C. Stuart, A. Fiser, R. Sanchez, F. Melo, A. Sali, Comparative protein structure modeling of genes and genomes, Annu. Rev. Biophys. Biomol. Struct. 29 (2000) 291–325.
[30] R.A. Laskowski, M.W. MacArthur, D.S. Moss, J.M. Thornton, PROCHECK: a program to check the stereochemical quality of protein structures, J. Appl. Cryst. 26 (1993) 283–291.
[31] Binding-Site User Guide, Accelrys, San Diego, MSI, USA, 1999.
[32] J. Gasteiger, M. Marsili, Iterative partial equalization of orbital electronegativity. A rapid access to atomic charges, Tetrahedron 36 (1980) 3219–3228.
[33] M.J.S. Dewar, E.G. Zoebisch, E.F. Healy, J.J.P. Stewart, AM1: a new general purpose quantum mechanical molecular model, J. Am. Chem. Soc. 107 (1985) 3902–3909.
[34] J. Stamos, M.X. Sliwkowski, C. Eigenbrot, Structure of the epidermal growth factor receptor kinase domain alone and in complex with a 4-anilinoquinazoline inhibitor, J. Biol. Chem. 277 (2002) 46265–46272.
[35] A. Wissner, M.B. Brawner Floyd, S.K. Rabindram, R. Nilakantan, L.M. Greenberger, R. Shen, Y.F. Wang, H.R. Tsou, Syntheses and EGFR and HER-2 kinase inhibitory activities of 4-anilinoquinoline-3-carbonitriles: analogues of three important 4-anilinoquinolines currently undergoing clinical evaluation as therapeutic anti-tumor agents, Bioorg. Med. Chem. Lett. 12 (2002) 2893–2897.
[36] J.H. Atkins, L.J. Gershell, Selective anticancer drugs, Nat. Rev. Drug Discov. 1 (2002) 491–492.
[37] L. Shewchuk, A. Hassell, B. Wisely, W. Rocque, W. Holmes, J. Veal, L.F. Kuyper, Binding mode of the 4-anilinoquinazoline class of protein kinase inhibitor: X-ray crystallographic studies of 4-anilinoquinazolines bound to cyclin-dependent kinase 2 and p38 kinase, J. Med. Chem. 43 (2000) 133–138.
[38] G.W. Rewcastle, W.A. Denny, A.J. Bridges, H. Zhou, D.R. Cody, A. McMichael, D.W. Fry, Tyrosine kinase inhibitors. 5. Synthesis and structure–activity relationships for 4-[(phenylmethyl) amino]- and 4-(phenylamino)quinazolines as potent adenosine 5′-triphosphate binding site inhibitors of the tyrosine kinase domain of the epidermal growth factor receptor, J. Med. Chem. 38 (1995) 3482–3487.